Environmental Technology & Innovation 42 (2026) 104908

Contents lists available at ScienceDirect

Environmental Technology & Innovation

journal homepage: www.elsevier.com/locate/eti

Melt-blended biodegradable mulching films with zeolite fillers from industrial by-products: A scalable, solvent-free route for controlled zinc delivery

Giulio Galamini [a,1], Andrea Saccani [b,1], Laura Sisti [b,*], Daniele Malferrari [a,c,**], Carmen Minichiello [b], Micaela Vannini [b], Luisa Barbieri [c,d]

[a] Department of Chemical and Geological Sciences, University of Modena and Reggio Emilia, Via G. Campi 103, Modena 41125, Italy
[b] Department of Civil, Chemical, Environmental and Materials Engineering, University of Bologna, Via Terracini 28, Bologna 40131, Italy
[c] Biogest-Sitea, Piazzale Europa 1a, Reggio Emilia 42124, Italy
[d] Engineering Department "Enzo Ferrari", University of Modena and Reggio Emilia, Via P. Vivarelli 10, Modena 41125, Italy

ARTICLE INFO

Keywords:
Mulching film
Biopolymer
Zeolite
Micronutrients
Zinc

ABSTRACT

To produce functionalized mulching films with added agronomic benefits, poly(butylene succinate-*co*-adipate) (PBSA) composites were developed by incorporating small amounts (2–4 wt%) of two different zeolitic tuffs through melt compounding. One of the zeolitic tuffs, sourced as by-product of quarrying operations, was enriched in zinc ions (Zn^{2+}) by cation-exchange process, enabling the zeolite to act as a reservoir of an essential micronutrient for plant growth. All the composite films were characterized in terms of mechanical and thermal properties to evaluate their suitability for agricultural applications, where flexibility and thermal stability are critical. Among the tested formulations, PBSA composites containing 4 wt% chabazite-rich zeolitic tuff exhibited good mechanical performance, with suitable elongation at break values. The addition of polyethylene glycol (PEG) enhanced filler dispersion, thereby preserving the mechanical properties of the composite. Kinetic release studies on composite granules and film demonstrated a controlled release of Zn^{2+}, with values of 14.9 ± 1.91 mg/kg and 9.33 ± 1.56 mg/kg for the material in granular and film forms, respectively, after 96 h of extraction. Overall, the results support the development of biodegradable mulching films that combine mechanical robustness with functional agronomic benefits, potentially contributing to more sustainable and efficient agricultural practices through weed suppression, soil protection, and micronutrient enrichment.

1. Introduction

The ongoing growth of the global population, combined with the progressive depletion and degradation of arable land, is exerting increasing pressure on agricultural systems to enhance productivity in a sustainable way. One of the most effective strategies is the use of mulching films, which have demonstrated a significant positive impact on crop performance (Akhir and Mustapha, 2022). Despite

* Corresponding author.
** Corresponding author at: Department of Chemical and Geological Sciences, University of Modena and Reggio Emilia, Via G. Campi 103, Modena 41125, Italy.
E-mail addresses: laura.sisti@unibo.it (L. Sisti), daniele.malferrari@unimore.it (D. Malferrari).
[1] These Authors contributed equally

https://doi.org/10.1016/j.eti.2026.104908
Received 9 December 2025; Received in revised form 5 March 2026; Accepted 24 March 2026
Available online 25 March 2026

concerns regarding their environmental impact (Steinmetz et al., 2016), mulching films are widely recognized for their ability to improve soil hydrothermal conditions, suppress parasitic weeds, limit soil erosion, and ultimately increase crop yield. However, the environmental drawbacks of conventional mulching films are mainly associated with their composition. In fact, most are produced from petroleum-derived, non-biodegradable polymers and often contain synthetic industrial additives (Bao et al., 2024; Salama and Geyer, 2023; Tang, 2023; Khalid et al., 2023; Scopetani et al., 2025). Residual fragments of these materials can persist in the soil after use, contributing to long-term contamination and potentially impairing soil health. Even when removed post-harvest, polyethylene-based films are often heavily soiled and degraded, making recycling technically challenging and economically unfeasible (Yu et al., 2024). In this context, biopolymers have emerged as a promising alternative for the production of environmentally friendly mulching films (Serrano-Ruiz et al., 2021; Mansoor et al., 2022). Due to their biodegradability in soil, biopolymers, bio-copolymers, and their blends are gaining interest as sustainable solutions (Miles et al., 2017; Dong et al., 2022; de Sousa et al., 2021; Parida et al., 2022). Biodegradable mulching films have been associated with augmented microbial diversity and activity (Paliaga et al., 2025; Zhang et al., 2024), parameters that are recognized as soil quality indicators in the framework of the European Green Deal (Orgiazzi et al., 2022). Furthermore, to reduce production costs, still higher than those of conventional plastics, composite formulations incorporating agro-industrial residues as fillers have been investigated (Pagliarini et al., 2023; Zhang et al., 2025; Sahoo and Rout, 2024; Merino et al., 2022).

Among currently available biodegradable polymers for agricultural mulching films poly(butylene succinate-*co*-adipate) (PBSA) offers a particularly favorable balance between mechanical performance and soil biodegradability. Compared to polylactic acid (PLA), PBSA exhibits significantly higher flexibility and elongation at break values, resulting in mechanical behavior closer to that of conventional polyethylene mulches and improved resistance to cracking during installation and field use. Moreover, PBSA is able to biodegrade under typical soil conditions, whereas PLA shows limited degradation at ambient temperatures and generally requires industrial composting conditions to undergo effective hydrolysis. These limitations restrict the suitability of neat PLA for in-soil applications, despite its high stiffness and bio-based origin. In comparison with polyhydroxyalkanoates (PHAs), PBSA presents more consistent processability and mechanical stability in film applications. Although PHAs are fully bio-based and readily biodegradable in soil, many PHA grades exhibit brittleness, narrow processing windows, and high production costs, which currently limit their large-scale adoption in agricultural mulching. PBSA, as a flexible aliphatic copolyester, allows tunable crystallinity and degradation rates through copolymer composition, enabling the design of mulch films with controlled service life aligned with crop cycles. Overall, PBSA represents a technically robust and economically viable alternative to PLA and PHA for biodegradable mulch films, particularly where mechanical durability during cultivation and reliable soil biodegradation after use are required (Abbate et al., 2023).

Beyond biodegradability, further advances in mulching films can be made by functionalizing them to act as smart delivery systems. Incorporating active functionalities such as the controlled release of nutrients or pesticides can significantly enhance agricultural sustainability. During the growing season and especially at the end, once the films are incorporated into the soil, they slowly enrich the soil with the functionalizing molecule, avoiding local toxicity and losses. Among nutrients, controlled delivery is particularly relevant for zinc, since zinc deficiency is widely reported in agricultural soils and the effectiveness of soil-applied zinc can be limited by rapid immobilization processes which reduce the concentration of readily available Zn^{2+} in the soil solution (Dhaliwal et al., 2022; Moreno-Lora and Delgado, 2020; Noulas et al., 2018). Beyond these agronomic issues, zinc also play an essential role in human health: zinc is a key element involved in numerous enzymatic functions, and its deficiency is recognized as a widespread nutritional problem, particularly in developing countries (Krężel and Maret, 2016; Younas et al., 2023). Chronic zinc deficiency can lead to irreversible cognitive and physiological impairments, especially in children (Cakmak and Kutman, 2018). Inadequate zinc intake is often associated with both low dietary diversity and poor zinc bioavailability in crops. It is, in fact, estimated that nearly half of the world's agricultural soils are zinc-deficient, ultimately resulting in lower levels of this micronutrient in edible crops (Liu et al., 2020).

Embedding a zinc carrier within a biodegradable mulching film offers potential agronomic advantages. Although the net effects are soil-specific (Kader et al., 2017), this approach may ensure a uniform distribution of the micronutrient across the soil-film interface, facilitating a sustained release throughout the cropping cycle. By synchronizing nutrient supply with crop demand, this system mitigates the risk of localized concentration peaks and streamlines field operations (Abbas et al., 2025; Priya et al., 2024). Unlike conventional soil broadcasting, which is prone to nutrient fixation, or weather-dependent foliar sprays, functional mulching films provide an integrated delivery platform that leverages an already established agricultural practice (Lateef et al., 2016; Correa et al., 2022; Pagliarini, et al., 2023). Various inorganic and organic micro- or nano-porous materials have been explored as carriers for active compounds like, for example, nutrients, pesticides and herbicides (Singh et al., 2022; Zhang et al., 2022, 2025). Incorporating a stable nutrient carrier, such as zeolitic tuffs, into biodegradable mulching films could be further interesting as this could enhance the slow-release effect (dos Santos Pereira et al., 2021). In fact, after film degradation and release of nutrients, zeolites remain in the soil, potentially providing long-term benefits by increasing soil cation exchange capacity (CEC) and water-holding capacity, while also mitigating soil greenhouse gas emissions associated with agricultural practices (Cataldo et al., 2021; Chen et al., 2025; Eslami et al., 2018; Jarosz et al., 2022; Morante-Carballo et al., 2021).

Zeolitic tuffs are naturally occurring rocks formed through the diagenetic transformation of volcanic ash. Their mineralogical composition varies depending on geological conditions, and they may contain up to 80 wt% of zeolite phases such as analcime, chabazite, clinoptilolite, mordenite, and phillipsite (Bish and Ming, 2001). Importantly, their use in agriculture does not necessarily require the development of new quarries. Instead, zeolite-rich by-products from existing quarrying operations, which are often discarded as waste, can be valorized for this purpose (Malferrari et al., 2013; Galamini et al., 2024). These by-products originate, for example, from sections of the quarry where the rock is naturally fractured and unsuitable for cutting into construction blocks (Faccini et al., 2015).

Recent research (Galamini et al., 2024) has shown that zeolitic tuffs in powder form can be effectively used for the controlled

release of zinc in soil. In the present paper, this feature is exploited to produce by direct melt mixing (i.e., without the use of solvents) composite compounds to be converted in advanced biodegradable mulching systems that promote circular economy through waste recycling, combining the benefits of weed suppression and soil conditioning with targeted nutrient delivery. By comparing a chabazite-rich tuff (ZECh, 68.5 wt% chabazite) with a phillipsite/chabazite-bearing tuff (ZEPh, 32.4 wt% phillipsite and 21.1 wt% chabazite), this study evaluated the hypothesis that divergent framework topologies (i.e., differences in channel dimensionality, pore connectivity, exchange-site accessibility, and crystal habits of different zeolitic species) affect: (i) the mechanical and physical incorporation of the zeolitic tuff into the PBSA matrix, (ii) the loading efficiency of Zn^{2+} during the ion-exchange, and (iii) the subsequent diffusion-mediated release of Zn^{2+} from the composite film.

While both chabazite and phillipsite share similar chemical compositions, being zeolites capable of exchanging cations, they differ significantly in their crystallographic structures, morphologies (crystal habit), and ion-exchange kinetics. Chabazite features large elliptical cages with 8-membered ring openings and forms pseudo-cubic or rhombohedral crystals with well-developed cleavage. Phillipsite, on the other hand, exhibits more disordered, non-uniform cages with anisotropic crystal growth, commonly forming monoclinic tabular crystals with less prominent cleavage (irregular to conchoidal fracture). Although their CEC are comparable (approximately 3.0–3.8 and 3.5–4.0 mEq/g for chabazite and phillipsite, respectively, their exchange kinetics may differ due to structural differences, pore size, and channel connectivity (Bish and Ming, 2001; Malferrari et al., 2013). The lower structural density and the more open, interconnected pore network of chabazite (three-dimensional channels interconnected via 8-rings) may facilitate faster ion exchange compared to the more tortuous and narrower channels in some directions of phillipsite (2D or pseudo-3D, but more anisotropic). Consequently, chabazite, due to its more open 3D pore connectivity, is expected to provide a faster Zn^{2+} loading and release. Conversely, while the tabular habit of phillipsite may enhance the mechanical incorporation of the filler into polymeric matrices, its anisotropic pore system likely constrains exchange-site accessibility and ion diffusion; this structural limitation may influence both the Zn^{2+} uptake efficiency during loading and the resulting kinetic profile of release.

These dynamics were evaluated using a series of PBSA-based composites prepared by melt blending the biopolymer with varying concentrations of either virgin or Zn-exchanged zeolitic tuffs. The composite formulations were optimized to balance mechanical integrity, filler dispersion, and functional performance. From the optimized batches, biodegradable films were fabricated and subjected to controlled laboratory tests to evaluate the release profile of zinc.

2. Materials and methods

2.1. Materials

The PBSA employed in this study is a commercial biopolymer BioPBSTM FD92PM, PTTMCC Biochem (Dusseldorf, Germany) characterized by the following composition $(PBS)_{0.7}$ – $(PBA)_{0.3}$ a glass transition temperature of −46 °C and a melting point of 85 °C.

Polyethylene glycol (PEG 6000), supplied by Sigma-Aldrich (St. Louis, MO, USA), was employed in the formulation as compatibilizer to enhance the dispersion of the inorganic filler within the polymer matrix. This grade of PEG has an average molecular weight of 3350 g/mol and a melting point in the range of 54–58 °C.

The chemical and mineralogical characterization of the two zeolitic tuffs, net of small differences that may exist between different samplings, is given in Malferrari et al. (2013) for ZECh (where it is referred to as Sorano) and in Supplementary material for ZEPh. Zinc loading was carried out as indicated in Galamini et al. (2024). Briefly, 50 mL of 0.1 M $ZnSO_4$-$6H_2O$ solution (previously acidified with a few drops of concentrated HNO_3 to facilitate solubilization) was added to 1.5 g of finely ground zeolitic tuff in closed PVF flasks and stirred at 400 rpm for 24 h at 20 °C. The suspension was then centrifuged at 6000 rpm for 4 min and the supernatant separated from the solid. The solid was then washed ten times with 50 mL of Millipore water each, stirred at 400 rpm for 5 min per wash, and the water was removed by centrifugation at 6000 rpm for 2 min. The resulting powder was air-dried and gently ground using an agate mortar. Infrared spectra before and after zinc loading were collected using an ATR FT-IR over the wavenumber range 650–4000 cm^{-1} using a

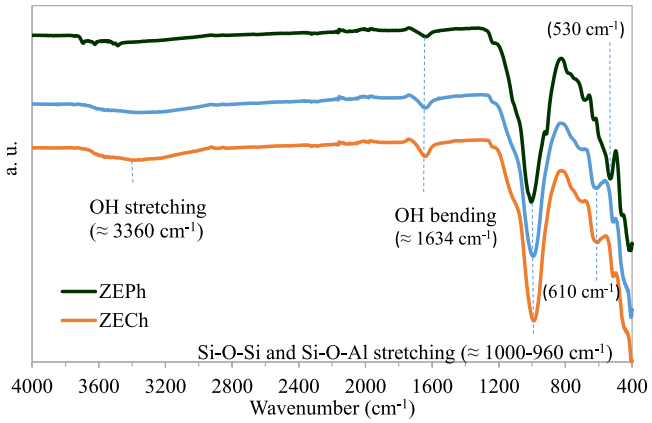

Fig. 1. FTIR spectra of virgin and Zn-exchanged zeolitic tuffs.

Perkin Elmer Spectrum Three FT-IR spectrometer equipped with a Universal ATR sampling accessory (Perkin Elmer Inc. MA, USA). Sixteen scans were taken for each spectrum at a resolution of 4 cm^{-1} and average results are reported in Fig. 1. The bands at 3360 and 1634 cm^{-1} are attributed to stretching and bending vibrations of the O-H group, respectively. The band between 1000 cm^{-1} and 960 cm^{-1} is characteristic of zeolite structures and is associated with the asymmetric stretching vibration of Si-O-Si and Si-O-Al. The signal around 685 cm^{-1} can be attributed to the symmetric stretching vibration of Si-O-Si, while the band at 601 cm^{-1} corresponds to the coupling vibration of the SiO_4 and AlO_4 tetrahedra. Moreover, the bands in the range of 800–500 cm^{-1}, in addition to being related to the Si-O and Al-O tetrahedral units, are associated to the sorption of metal cations. Notably, the FT-IR spectrum of the zinc-modified zeolite (ZECh(Zn)) showed no significant differences compared to the pristine material (ZECh), indicating that the zinc incorporation process used does not alter the zeolite framework.

As will be better explained in 3.1, ZEPh was not exchanged with zinc as the polymer filled with virgin ZEPh returned low strain at break values.

The thermal stability of the fillers, investigated by thermogravimetric analysis (TGA) using a TGA 55 Discovery model (TA Instrument, Delaware, USA) in nitrogen flow (40 mL/min), is reported in Fig. 2. Prior to analyses, the zeolitic tuffs were treated at 60 °C under vacuum for 12 h. As shown, the thermal behavior of the powders is similar, particularly in the zone of interest (below 130 °C), which correspond to the temperature range of the compounding process. Notably, the ion exchange does not alter the weight loss at low temperatures; however, the thermal treatment at 60 °C is not sufficient to completely remove moisture, leaving about 5 wt% residual humidity.

2.2. Composite manufacturing

Biocomposites were prepared by melt mixing using a Brabender compounder PL-2000 Plasti-Corder (Anton Paar, Graz, Austria). Batch compositions are reported in Table 1. Both PBSA pellets and zeolitic tuffs were previously dried at 60 °C under vacuum for 12 h to minimize moisture and avoid polymer degradation. After PBSA melting, PEG6000, when included as a compatibilizer, was added in powder form, maintaining a fixed PEG:zeolite mass ratio of 1:2 (Hongsriphan et al., 2019), with the aim of promoting the homogeneous dispersion of the inorganic phase within the polymer matrix. A PEG-free series was also prepared to evaluate its influence on filler dispersion. Subsequently, the zeolitic tuff powders were incorporated, and mixing was conducted for 4 min at 100 rpm and 130 °C under identical processing conditions for all formulations.

Composite production and characterization were conducted in incremental steps, guided by performance test feedback. Consequently, as better detailed in 3.1, only select combinations were prepared, rather than all possible permutations.

For the characterizations, the obtained composites were cryogenically ground using liquid nitrogen to obtain fine granules suitable for further processing. Dog-bone specimens, compliant with ISO 527–2 Type 1BA, were produced via injection molding using a Babyplast 6/12 injection moulder (Rambaldi Group, Molteno (LC), Italy) for mechanical testing. Additionally, films with a thickness of 200 ± 20 μm were prepared through compression molding and submitted to further testing.

2.3. Composite characterizations

The molecular weight distribution of the polymer samples after the compounding process was investigated by Gel Permeation Chromatography (GPC), model Azura HP 1100 (KNAUER, Berlin, Germany) equipped with a PL gel 5 μm Minimixed-C column, a refractive index detector, using as solvent and as eluting phase $CHCl_3$ at 30 °C and 0.3 mL/min flow. A calibration plot was constructed with monodisperse polystyrene standards.

TGA was operated in nitrogen atmosphere for all samples, using the previously described instrument at a 10 °C min^{-1} heating rate from 50 to 800 °C and a gas flow of 30 mL min^{-1}. The onset degradation temperatures (T_{onset}) were taken from the intersection of the

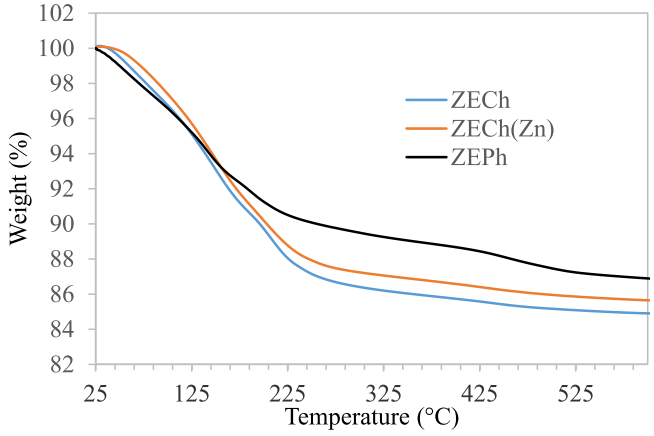

Fig. 2. TGA of virgin and Zn-exchanged zeolitic tuffs.

Table 1
Tags and composition of the investigated composites.

Sample	PBSA (wt%)	Zeolitic tuff (wt%)	PEG (wt%)
PBSA	100	0	0
PBSA/ZECh2	98	2	0
PBSA/ZECh4	96	4	0
PBSA/PEG	99	0	1
PBSA/PEG/ZECh2	97	2	1
PBSA/PEG/ZECh4	94	4	2
PBSA/PEG/ZEPh4	94	4	2
PBSA/PEG/ZECh(Zn)4	94	4	2

tangents between the initial point and the inflection point, T_{max} were calculated as the temperature of the maximum degradation rate, while $T_{5\%}$ were determined as the temperature at which 5% weight loss was reached.

Differential scanning calorimetry was carried out by means of a TA Q10 DSC (TA Instrument, Delaware, USA) in nitrogen flux (20 mL/min) at 10 °C min^{-1} rate. The following scan sequences were applied: heating from 30 to 170 °C at 10 °C min^{-1}, holding for 1 min to erase the previous thermal history, cooling from 170 to −60 °C at 10 °C min^{-1}, holding at −60 °C for 3 min and last scan heating up to 170 °C at the same rate. Integrating the melting peak of the last scan and assuming a melting enthalpy of the crystalline phase (ΔH_m^0) of 116.9 J g^{-1} (Minichiello et al., 2025), the crystallinity index (CI) of the tested samples was derived according to Eq. (1):

$$CI\ (\%) = \frac{\Delta H_m}{f \cdot\ \Delta H_m^0} \cdot\ 100 \tag{1}$$

where f is the amount of polymer fraction in the samples.

To evaluate the flexibility of the developed materials for potential application as mulching films, their mechanical properties were assessed. The tensile properties of neat PBSA and its composites were measured at T = 25 ± 1 °C and a strain rate of 50 mm/min by means of an INSTRON 5966 series test apparatus (INSTRON, Pianezza (TO), Italy) equipped with a 10 kN load cell, without applying a preload according to the standard ISO 527–1. At least five specimens for each composition were tested. The software reported the stress–strain graphs for each composition and calculated the value of Young's modulus according to the slope of linear part of these curves without the use of an extensometer.

The brittle fracture surfaces of the dog-bone specimen relevant to the most promising compositions were observed by scanning electron microscopy (XL 20 Philips, FEI, Hillsboro, OR, USA) after gold metallization by means of a Quorum 150 R ES (Quorum Technologies Ltd., East Sussex, UK).

Zn^{2+} release over time was evaluated in 0.01 M $CaCl_2$ as a standardized unbuffered electrolyte, commonly used in soil chemistry to approximate soil-solution ionic strength and to estimate the readily exchangeable metal fraction under controlled conditions. Therefore, the obtained values are mainly indicative of exchangeable Zn and of the characteristics of the exchange complex (Conti et al., 2000; Houba et al., 2000; Kaur et al., 2024; Pueyo et al., 2004). However, this simplified medium does not reproduce the full complexity of soil environments (e.g., variable pH, dissolved organic matter, heterogeneous sorption sites and multi-ion competition), and therefore the measured release profiles should be interpreted as potential Zn^{2+} release under controlled ionic strength rather than as direct field predictions. The tests were carried out both on the granular material and on films.

Kinetic tests were performed for PBSA/PEG/ZE(Zn)4 with three replicates per sample. For both granules and films, 0.2 g of material was placed in contact with 10 g of the extracting solution in closed centrifuge tubes. The mulching film was initially cut into 1 × 1 cm squares. Then, the supernatant was separated at different time points (3, 6, 18, 24, 48, and 96 h) and filtered with 0.2 μm nylon syringe filters. The separated liquid was acidified by adding 0.1 g of HNO_3 (this slight dilution was accounted for in the subsequent calculations). The samples were analyzed with an ICP-MS (model: Thermo Fisher Scientific, Waltham, MA, USA). Kinetic modelling was performed without using linearization to avoid parameter estimation bias (Wang et al., 2024). For each time points, the mean value of the three replicates (q_t) was used in the fitting procedure. Kinetic modelling was performed in R Studio with PUPAK package (Magalong et al., 2022).

The release of Zn^{2+} from PBSA/PEG/ZECh(Zn)4 was evaluated till the maximum tested time (96 h) for both granular and film samples and compared with the zinc-depleted material (PBSA/PEG/ZECh4) as well as the material without zeolitic tuff (PBSA/PEG). Three replicates were used for each sample. To assess the significance of the differences observed in Zn^{2+} release ($p < 0.05$), parametric tests including Analysis of Variance (ANOVA) and Tukey's HSD were applied to data meeting the assumptions of normality and homoscedasticity (verified through Shapiro–Wilk and Bartlett tests). For datasets that did not meet these assumptions, the non-parametric Kruskal–Wallis test was used. Statistical analyses were performed with R Studio, with the Agricolae and MASS packages (de Mendiburu, 2006; Venables and Ripley, 2002, respectively).

Table 2
DSC results of the investigated materials.

Sample	T_m (°C)*	ΔH_m (J/g)*	T_c (°C)^	ΔH_c (J/g)^	T_g (°C)*	CI (%)
PBSA	87	49	36	49	-47	42
PBSA/ZECh2	87	49	37	49	-46	43
PBSA/ZECh4	87	49	37	49	-46	44
PBSA/PEG	87	51	37	50	-46	44
PBSA/PEG/ZECh2	86	49	37	49	-46	44
PBSA/PEG/ZECh4	86	49	39	49	-47	45
PBSA/PEG/ZEPh4	87	48	38	48	-47	44
PBSA/PEG/ZECh(Zn)4	87	48	37	47	-47	44

*From the third heating scan, ^ from the second cooling scan

Table 3
TGA results of the investigated materials.

Sample	T_{onset} (°C)	T_{max} (°C)	$T_{5\%}$ (°C)	Residue* (%)
PBSA	360	408	361	1
PBSA/ZECh2	359	392	345	2
PBSA/ZECh4	352	384	346	4
PBSA/PEG	357	390	351	1
PBSA/PEG/ZECh2	354	394	344	2
PBSA/PEG/ZECh4	353	390	349	4
PBSA/PEG/ZEPh4	352	383	346	4
PBSA/PEG/ZECh(Zn)4	347	382	342	4

*Measured at 700°C

3. Results and discussion

3.1. Filler and PEG effect on material properties

To gain deeper understanding of how the material composition affects overall performance, the thermal and mechanical properties of the composites were thoroughly investigated. Particular attention was given to understand the role of the zeolitic tuff filler and the addition of PEG, in order to assess their influence on key thermal transitions and structural features. For this purpose, composites containing varying amounts of ZECh and PEG were initially prepared (Table 1) and, after determining that 4 wt% was the optimal zeolitic tuff dosage and that 2 wt% PEG addition improved performance, the ZEPh composite was prepared exclusively at these optimal concentrations (sample PBSA/PEG/ZEPh4, Table 1). However, since this material failed subsequent mechanical tests, the corresponding zinc-exchanged ZEPh composite was not prepared. Instead, the focus was posed solely on that with ZECh (PBSA/PEG/ZECh(Zn)4, Table 1).

Notably, the effects of zeolitic tuff and PEG were first evaluated with respect to the thermal behavior of the materials (Table 2) by DSC. In all specimens, the glass transition (T_g) and melting temperatures (T_m) remained essentially unchanged. Regarding the crystallization process, both PEG and the zeolitic tuff exhibited a slight nucleating effect, though acting in a non-synergistic manner, as indicated by a modest increase in the crystallization temperature (T_c) and the crystalline index (CI). This enhancement is not expected

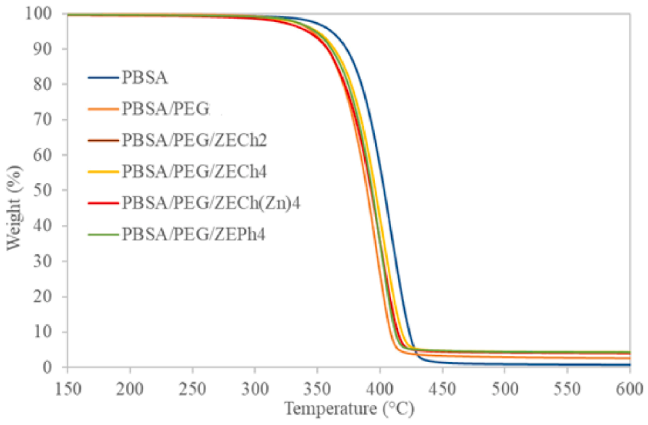

Fig. 3. TGA of some selected materials.

Table 4
GPC results of selected materials.

Sample	M_n (g/mol)	M_w (g/mol)	D*
PBSA	49300	84500	1.7
PBSA/ZECh4	40700	88000	2.2
PBSA/PEG	41000	86500	2.1
PBSA/PEG/ZECh4	42800	92900	2.2
PBSA/PEG/ZECh(Zn)4	40500	89500	2.2

*Polidispersity index

Table 5
Mechanical properties of the investigated materials.

Sample	Young Modulus (MPa)	Stress at break (MPa)	Strain at break (%)
PBSA	298 ± 5	17.8 ± 1.7	383 ± 21
PBSA/ZECh2	332 ± 5	14.9 ± 1.6	225 ± 15
PBSA/ZECh4	331 ± 12	12.7 ± 1.4	180 ± 11
PBSA/PEG	307 ± 2	17.9 ± 1.2	355 ± 23
PBSA/PEG/ZECh2	325 ± 5	16.7 ± 1.5	259 ± 16
PBSA/PEG/ZECh4	282 ± 30	16.8 ± 1.4	262 ± 12
PBSA/PEG/ZEPh4	280 ± 24	15.8 ± 0.7	211 ± 34
PBSA/PEG/ZECh(Zn)4	275 ± 28	14.3 ± 0.8	250 ± 8

to significantly affect the degradation rate of the PBSA matrix once the polymer is dispersed in soil, as observed in other materials (de Souza Vieira et al., 2021; Soulis et al., 2012).

The parameters related to the thermal stability, investigated by TGA under nitrogen atmosphere, are summarized in Table 3 while the thermograms are depicted in Fig. 3. Both the presence of the filler and PEG influence the thermal stability of the composites. In fact, both the T_{onset} and the $T_{5\%}$ are reduced, but they still remain well above the polymer processing temperature (130 °C) implying a negligible effect on polymer properties. Regarding the effect of the zinc ions, which are known to decrease the polymers thermal stability (Li et al., 2015; Klun and Krzan, 2003), it is again relatively limited, an indication that the Zn^{2+} cations are effectively entrapped within the structural channels of the zeolite, thereby minimizing their diffusion into the polymer matrix during compounding and subsequent processing steps. Additionally, the final residue increases with the rising of filler content, indicating a proportional contribution of the inorganic fraction to the overall thermal stability of the composites.

The potential degradation of PBSA in contact with the filler during the compounding stage was evaluated by GPC for the compositions with higher filler loading of ZECh. The molecular weight data reported in Table 4 show that the average molecular weights (M_w) of the samples containing the zeolitic tuff are comparable to those of the unloaded matrix after melt mixing. Although a slight increase in polydispersity is observed in all samples, indicating some rearrangement in the molecular weight distribution, no evidence of degradation process can be identified despite the presence of a small amount of water in the fillers (see Fig. 2).

The mechanical properties of the investigated samples are reported in Table 5. As can be observed, the effect of the filler on the elastic modulus is relatively limited in the samples (± 10%). From the DSC results also the effect of increased crystallinity can be ruled out. More significant is the effect on the other parameters. Without the presence of PEG the dispersion of the filler leads to a marked decrease in both stress and strain at break. While the addition of PEG alone does not change the properties of neat PBSA, but it effectively mitigates the embrittlement of the composites, even at the highest filler content. Notably, the polar groups of PEG can promote the homogeneous dispersion of the inorganic filler by enhancing polymer–filler interfacial compatibility and preventing particle aggregation. This bridging action between the polar filler surface and the polymer matrix may contribute to reducing interfacial defects (Bendahou et al. 2015). This allows the strain at break to remain above 250%, but only in case of ZECh filler. For this reason, the use of the ZEPh filler was abandoned in the last part of the research, due to the lower elongation at break values observed for the corresponding composites and their relatively higher standard deviation (more than double of the relative chabazite composite). This mechanical behaviour could be attributed to the tabular morphology of phillipsite particles. Although such a morphology could theoretically favor alignment within the polymer film, in practice it can lead to an uneven dispersion and the formation of preferential aggregation zones. These inhomogeneities likely acted as stress concentration points, promoting premature failure under tensile deformation and resulting in reduced ductility and higher data variability. Moreover, despite a slightly lower stress at break compared to PBSA/PEG/ZECh4, the final, targeted formulation, PBSA/PEG/ZECh(Zn)4, still maintains high elongation.

The microstructure of the samples with the highest tuff amount (4 wt%) is compared in Fig. 4. Although no remarkable differences are observed, in the samples formulated without PEG, an imperfect adhesion of the inorganic phase to the polymer matrix is visible (Fig. 4 left) leading to the presence of large porosities at the interphase. In the other two samples, an effective interaction/adhesion between the phases takes place but larger particles are found in the ZEPh samples (Fig. 4 centre) than in ZECh samples (Fig. 4 right) a feature that can explain the reduced plastic deformation of the former composition.

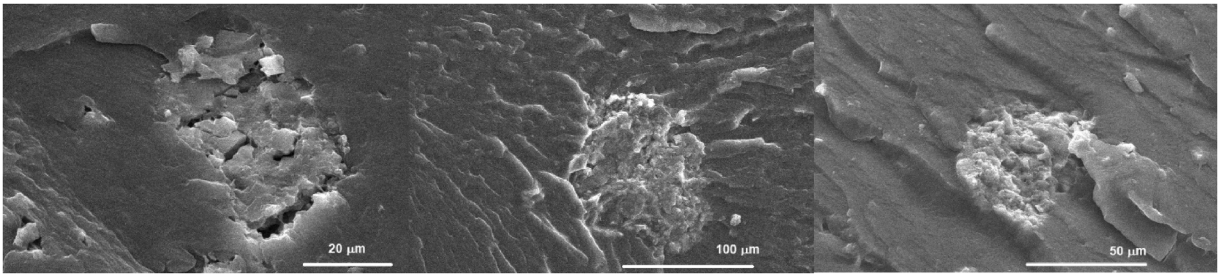

Fig. 4. Microstructure of samples PBSA/ZECh4 (left), PBSA/PEG/ZEPh4 (centre) and PBSA/PEG/ZECh4 (right).

3.2. Release kinetic of Zn^{2+}

The time-dependent release of Zn^{2+} was evaluated in a 0.01 M $CaCl_2$ solution, to simulate soil pore water and assess zinc availability under conditions relevant to practical application (Conti et al., 2000; Houba et al., 2000). As established in 2.3, while 0.01 M $CaCl_2$ serves a reproducible background electrolyte to compare formulations, Zn^{2+} availability in natural soil environments are subject to a multitude of competing physicochemical processes that may lead to divergent behavior. Soil pH can alter zinc speciation and solubility and can shift the balance between exchangeable and adsorbed pools (Sanders and El Kherbawy, 1987). In addition, the soil organic matter may complex zinc and modify its activity either promoting zinc mobilization (by complexation-driven desorption) or reducing its bioavailability (Cheng and Allen, 2006). Competing cations typical of soil solutions (e.g., Ca^{2+}, Mg^{2+}, K^+, NH_4^+, Na^+) may affect

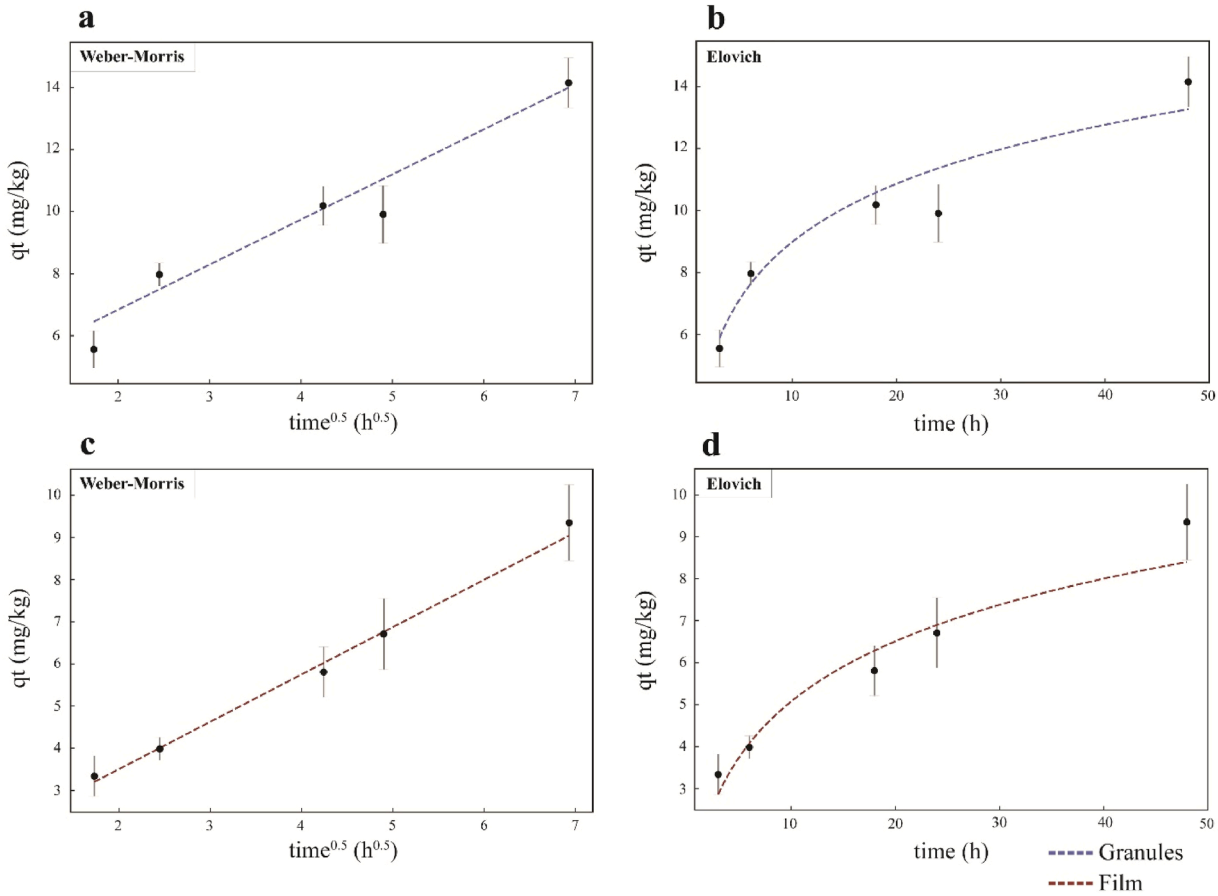

Fig. 5. Representation of the best-fitting kinetic models as Elovich [q_t (mg $Zn^{2+}kg^{-1}$) vs. time (h)], and Weber–Morris [qt (mg $Zn^{2+}kg^{-1}$) vs. time$^{0.5}$ ($h^{0.5}$)] for the release of Zn^{2+} from PBSA/PEG/ZECh(Zn)$_4$. (A) Weber–Morris model for granules, (B) Elovich model for granules, (C) Weber–Morris model for mulching films, and (D) Elovich model for mulching films. Data points represent the mean of replicates, and the standard errors of the mean (SEM) are shown as error bars. Film-like specimens exhibited a lower cumulative Zn^{2+} release than granules, consistent with polymer-matrix mass-transfer limitations that reduce the early-time release contribution.

competitive exchange on zeolite sites and influence diffusion gradients, thereby changing both the extent and the kinetics of zinc release compared with the $CaCl_2$-only system (Inglezakis et al., 2005). Finally, agricultural practices and land management changes (e.g., organic vs. mineral fertilization, tillage regime, etc.) induce significant modifications in the soil ecosystem and physicochemical properties, affecting the availability of zinc and micronutrients in general (Herencia et al., 2011; de Santiago et al., 2008).

For these reasons, the kinetic trends observed here are discussed as comparative performance under controlled ionic strength, and further validation under representative soil conditions is required to translate these results into agronomic release scenarios. Release behavior was analyzed for both granular material and PBSA-based films. As a matter of fact, the release mechanism could be driven by multiple processes evolving over time. In the early stages, when the polymer matrix is still structurally intact, Zn^{2+} release is driven by ion-exchange processes between Zn^{2+} immobilized in the modified zeolitic tuffs and the ions present in the surrounding medium. As PBSA degradation progresses, the increase in matrix porosity and the loss of structural continuity enhance the exposure of the zeolitic phase and facilitate Zn^{2+} diffusion (Minichiello et al., 2025). Consequently, polymer matrix degradation becomes a key factor controlling Zn^{2+} release at later stages. The plot of the release of Zn^{2+} (mg kg^{-1}) by PBSE/PEG/ZECh(Zn)4 in granule or film form, is shown in Fig. 5, where are reported the two best fitting models (Weber–Morris intraparticle diffusion and Elovich). The minimal difference between q_t at 48 h and 96 h suggests that near-equilibrium conditions were reached within the first 48 h. The data point at 96 h was therefore not included in the kinetic modeling. Statistical and kinetic parameters of the four best fitting models are reported in Tables 6 and 7, respectively, for the release of Zn^{2+} (mg/kg) by PBSA/PEG/ZECh(Zn)4 in granule and film form.

Among the models tested, Weber–Morris provided the best description of the Zn^{2+} release from PBSA/PEG/ZECh(Zn)4 for both mulching film and granules, with the highest R^2 values and the lowest AIC. The Elovich model also described the release kinetics well, confirming its relevance in representing the release behavior.

Weber–Morris intraparticle diffusion is represented by Eq. (2) (Wu et al., 2009):

$$q_t = k_{ID} t^{0.5} + C \tag{2}$$

where, in this context of release kinetics, q_t is defined as the Zn^{2+} release capacity at time t (mg Zn^{2+} kg^{-1}) or time-dependent release capacity, k_{ID} is the intraparticle diffusion constant (mg kg^{-1} $h^{-0.5}$), t is time ($h^{0.5}$), and C is a constant related the boundary layer effect in the diffusion of Zn^{2+} outside the material. Specifically, C represents the resistance to surface diffusion. When C = 0, intraparticle diffusion can be assumed to be the sole rate-limiting mechanism, with no boundary layer effects.

Although the Elovich model was originally developed for chemisorption, it has also shown good predictive capacity in ion-exchange systems such as zeolites (e.g., Noroozifar et al., 2014). Elovich equation is reported in Eq. (3) (Qiu et al., 2009):

$$q_t = \frac{1}{\beta}\ln(1 + \alpha\beta t) \tag{3}$$

where q_t is the Zn^{2+} release capacity at time t (mg Zn^{2+} kg^{-1}), t is time (h), α is the initial Zn^{2+} releasing rate (mg Zn^{2+} kg^{-1} h^{-1}), and β is the desorption constant (kg mg^{-1}). Specifically, β is related to the rate at which the Zn^{2+} release declines from the maximum initial value, determined by α.

The Elovich model suggests that the release of Zn^{2+} by PBSA/PEG/ZECh(Zn)4 was governed by heterogeneous interactions where the activation energy changes as a function of the surface coverage (β). Zeolites have a heterogeneous structure, which is likely even more pronounced in natural materials such as the zeolitic tuff used. Specifically, it is recognized that surface heterogeneity in zeolites results from: i) structurally different channels and cages, ii) crystal growth-related defects, and iii) hydroxyl groups heterogeneity (Datka et al., 1995). Moreover, Wennmacher et al. (2020) found that unequal distribution of aluminum not only caused uneven distribution of physicochemical characteristics in zeolites but also produced distinct habitus of the mineral.

The Weber–Morris model suggests the occurrence of diffusional constraints, as confirmed by the positive intercept C values, especially for granules. In systems controlled solely by internal diffusion, the intercept C is equal to zero. Conversely, C is higher than zero if the boundary layer plays a significant role as a limiting factor (limited film diffusivity), namely, when there is significant resistance to the external mass transfer. In this study, C is positive, indicating that the release of Zn^{2+} into the aqueous phase was affected by the boundary layer, especially for granules.

The Elovich model showed α values remarkably high compared to the highest q_t measured (q_t at 96 h: 14.9 ± 1.9 and 9.33 ± 1.56 mg kg^{-1} for granules and mulching film, respectively). The initial release of Zn^{2+} was therefore rapid; moreover, the granules exhibited a higher initial release rate compared to the mulching film. The relatively high values of β, which represent the rate at which the initial Zn^{2+} release rate (α) declines over time, indicate that the release rapidly decreased, indicating potential for slow releasing.

Overall, kinetic modelling suggests the occurrence of multiple rate-limiting processes, which is consistent with ion-exchangers, such as zeolites (Noroozifar et al., 2014). Beyond the goodness-of-fit, the lower cumulative Zn^{2+} release measured for the film specimens (9.33 ± 1.56 mg kg^{-1} at 96 h) compared with granules (14.9 ± 1.9 mg kg^{-1}) can be rationalized by additional mass-transfer constraints imposed by the polymer matrix. In film-like samples, a larger fraction of the zeolitic tuff is effectively encapsulated within PBSA; therefore, Ca^{2+}/electrolyte access to ion-exchange sites and the subsequent outward diffusion of released Zn^{2+} require transport through (or along) the polymer phase. This polymeric barrier is expected to reduce both the extent and the apparent rate of release within the investigated timeframe (Govil et al., 2024). Conversely, the granule morphology typically features a higher proportion of exposed or near-surface filler at fragmented faces and surface irregularities. This facilitates more rapid exchange at the solid/liquid interface, providing greater site accessibility and resulting in a significantly higher cumulative release. Within the Weber–Morris framework, the higher intercept C observed for granules (3.94 vs 1.25 mg kg^{-1}) is consistent with a greater contribution from fast release occurring at readily accessible surface/near-surface sites. In contrast, the lower C value for the films reflects a smaller

Table 6
Statistical parameters of the best fitting kinetic models for the release of Zn^{2+} in simulated soil water by PBSA/PEG/ZECh(Zn)4 in powder and film form. The acronyms are: RMSE (Root Mean Square Errors), MAE (Mean Absolute Error), and AIC (Akaike Information Criterion). R^2 refers to the linearizations of the Elovich, Pseudo 1st order, and Pseudo 2nd order models, or to the linear Weber–Morris model.

	Models	R^2	RMSE	MAE	AIC
Granules	Weber–Morris	0.936	0.687	0.552	0.251
	Elovich	0.939	0.809	0.678	1.88
	Pseudo-second-order	0.896	1.08	0.853	4.81
	Pseudo-first-order	0.807	1.44	1.13	7.63
Film	Weber–Morris	0.993	0.180	0.146	-13.1
	Elovich	0.939	0.529	0.437	-2.36
	Pseudo-second-order	0.870	0.771	0.639	1.40
	Pseudo-first-order	0.757	1.05	0.854	4.51

Table 7
Kinetic parameters for the release of Zn^{2+} in simulated soil water by PBSA/PEG/ZE(Zn)4.

	Models	Kinetic parameter 1		Kinetic parameter 2	
Granules	Weber–Morris	k_{ID} (mg kg^{-1} $h^{-0.5}$)	1.45	C (mg kg^{-1})	3.94
	Elovich	α (mg kg^{-1} h^{-1})	6.79 ± 2.17	β (kg mg^{-1})	0.360 ± 0.047
	Pseudo-second-order	k_2 (kg mg^{-1} h^{-1})	0.0161 ± 0.0037	q_e (mg kg^{-1})	13.7 ± 0.8
	Pseudo-first-order	k_1 (h^{-1})	0.194 ± 0.022	q_e (mg kg^{-1})	11.6 ± 0.5
Film	Weber–Morris	k_{ID} (mg kg^{-1} $h^{-0.5}$)	1.12	C (mg kg^{-1})	1.25
	Elovich	α (mg kg^{-1} h^{-1})	1.93 ± 0.57	β (kg mg^{-1})	0.446 ± 0.084
	Pseudo-second-order	k_2 (kg mg^{-1} h^{-1})	0.0142 ± 0.0048	q_e (mg kg^{-1})	9.25 ± 0.98
	Pseudo-first-order	k_1 (h^{-1})	0.131 ± 0.021	q_e (mg kg^{-1})	7.46 ± 0.59

surface-accessible fraction and the introduction of a secondary rate-controlling step (i.e., diffusion through the polymer matrix) which attenuates the early-stage release (Wu et al., 2009).

4. Conclusions

In this study, PBSA-based composites incorporating zeolitic tuff fillers by melt mixing were developed and evaluated for potential use in biodegradable mulching films. The incorporation of PEG played a key role in enhancing polymer-filler interfacial compatibility, thereby preserving the mechanical integrity of the films even at higher filler loadings. Among the formulations tested, the addition of 4 wt% of chabazite-rich zeolitic tuff proved particularly effective, enabling the production of films with satisfactory elongation at break values. In contrast, the incorporation of phillipsite-rich tuff resulted in diminished mechanical performance. This outcome is attributed to the tabular morphology of the crystals which, contrary to expectations, likely impeded uniform dispersion and weakened interfacial adhesion within the polymer matrix. Furthermore, the incorporation of Zn-loaded chabazite-rich zeolitic tuff enabled a sustained, gradual Zn^{2+} release under standardized conditions in 0.01 M $CaCl_2$, supporting the potential of these composites as functional biodegradable mulches for controlled micronutrient delivery. Nevertheless, these laboratory findings should be validated through field trials, where the effects of soil heterogeneity and environmental variables (e.g., pH fluctuations, cation competition, and organic ligands) can be fully accounted for. Overall, PBSA/PEG composites filled with Zn-exchanged chabazite-rich tuff represent a promising platform that combines mechanical reliability with added nutrient-release functionality.

CRediT authorship contribution statement

Andrea Saccani: Writing – original draft, Validation, Supervision, Resources, Investigation, Formal analysis, Data curation, Conceptualization. **Giulio Galamini:** Writing – review & editing, Validation, Investigation, Funding acquisition, Formal analysis. **Daniele Malferrari:** Writing – review & editing, Validation, Resources, Methodology, Funding acquisition. **Laura Sisti:** Writing – review & editing, Validation, Supervision, Resources, Methodology, Funding acquisition, Formal analysis, Data curation. **vannini micaela:** Validation, Supervision. **Carmen Minichiello:** Investigation, Funding acquisition, Formal analysis, Data curation. **Luisa Barbieri:** Writing – review & editing, Supervision, Methodology, Funding acquisition.

Funding

Authors wish to acknowledge Ecosister – “Ecosystem for Sustainable Transition in Emilia-Romagna”, project funded under the National Recovery and Resilience Plan (NRRP), Mission 04 Component 2 Investment 1.5 – NextGenerationEU, Call for tender n. 3277 dated 30/12/2021, Award Number: 0001052 dated 23/06/2022.

Declaration of Competing Interest

The authors declare that they have no known competing financial interests or personal relationships that could have appeared to influence the work reported in this paper.

Appendix A. Supporting information

Supplementary data associated with this article can be found in the online version at doi:10.1016/j.eti.2026.104908.

Data availability

Data will be made available on request.

References

Abbas, M., Depar, N., Ullah, S., Irfan, M., Shah, J.A., Afzal, J., 2025. Comparative efficacy of soil and foliar zinc application for agronomic biofortification of wheat with zinc. Discov. Soil 2, 121. https://doi.org/10.1007/s44378-025-00153-1.

Abbate, C., Scavo, A., Pesce, G.R., Fontanazza, S., Restuccia, A., Mauromicale, G., 2023. Soil bioplastic mulches for agroecosystem sustainability: a comprehensive review. Agricolture 13 (1), 197. https://doi.org/10.3390/agriculture13010197.

Akhir, M.A.M., Mustapha, M., 2022. Formulation of biodegradable plastic mulch film for agriculture crop protection: a review. Polym. Rev. 62, 890–918. https://doi.org/10.1080/15583724.2022.2041031.

Bao, H.X., Gu, Y., Chen, L., Wang, Z., Pan, H., Huang, S., Meng, Z., Chen, X., 2024. Microplastics derived from plastic mulch films and their carrier function effect on the environmental risk of pesticides. Sci. Total Environ. 924, 171472. https://doi.org/10.1016/j.scitotenv.2024.171472.

Bendahou, D., Bendahou, A., Grohens, Y., Kaddami, H., 2015. New nanocomposite design from zeolite and poly(lactic acid). In: Ind. Crops Prod, 72, pp. 107–118. https://doi.org/10.1016/j.indcrop.12.055.

Bish, D.L., Ming, D.W., 2001. Natural zeolites: occurrence, properties, applications, Reviews in mineralogy and geochemistry. Mineralogical Society of America, Washington, DC.

Cakmak, I., Kutman, U.B., 2018. Agronomic biofortification of cereals with zinc: a review. Eur. J. Soil Sci. 69, 172–180. https://doi.org/10.1111/ejss.12437.

Cataldo, E., Salvi, L., Paoli, F., Fucile, M., Masciandaro, G., Manzi, D., Masini, C.M., Mattii, G.B., 2021. Application of zeolites in agriculture and other potential uses: A review. Agronomy 11. https://doi.org/10.3390/agronomy11081547.

Chen, X., Liu, G., Liu, B., Chen, T., Li, Y., Chen, W., Pang, J., Siddique, K.H.M., Chi, D., 2025. Zeolite amendment enhances grain yield and mitigates greenhouse gas emissions in an intensive aerobic rice system. Field Crops Res. 327, 109884. https://doi.org/10.1016/j.fcr.2025.109884.

Cheng, T., Allen, H.E., 2006. Comparison of zinc complexation properties of dissolved natural organic matter from different surface waters. J. Environ. Manag. 80, 222–229. https://doi.org/10.1016/j.jenvman.2005.09.007.

Conti, A., Sacchi, E., Chiarle, M., Martinelli, G., Zuppi, G.M., 2000. Geochemistry of the formation waters in the Po plain (Northern Italy): an overview. Appl. Geochem 15, 51–65. https://doi.org/10.1016/S0883-2927(99)00016-5.

Correa, A.C., de Campos, A., Cunha Claro, P.I., Fernandes Guimaraes, G.G., Capparelli Mattoso, L.H., Marconcini, J.M., 2022. Biodegradability and nutrients release of thermoplastic starch and poly (ε-caprolactone) blends for agricultural uses. Carbohyd. Polym. 282, 119058. https://doi.org/10.1016/j.carbpol.2021.119058.

Datka, J., Boczar, M., Gil, B., 1995. Heterogeneity of hydroxyl groups in zeolites studied by IR spectroscopy. Colloids Surf. A Physicochem. Eng. Asp. A Sel. Pap. Presente 208th ACS Meet. Infrared Stud. Surf. Adsorbed Species 105, 1–18. https://doi.org/10.1016/0927-7757(95)03338-3.

Dhaliwal, S.S., Sharma, V., Shukla, A.K., Kaur, J., Verma, V., Kaur, M., Singh, P., Gaber, A., Hossain, A., 2022. Zinc-Based Mineral (ZnSO4·7H2O) and Chelated (Zn-EDTA) Fertilizers improve the Productivity, Quality and Efficiency Indices of Field Pea (Pisum sativum L.) through Biofortification. J. Trace Elem. Min. 2, 100033. https://doi.org/10.1016/j.jtemin.2022.100033.

Dong, H., Yang, G., Zhang, Y., Yang, Y., Wang, D., Zhou, C., 2022. Recycling, disposal, or biodegradable-alternative of polyethylene plastic film for agricultural mulching? A life cycle analysis of their environmental impacts. J. Clean. Prod. 380, 134950. https://doi.org/10.1016/j.jclepro.2022.134950.

Eslami, M., Khorassani, R., Coltorti, M., Malferrari, D., Faccini, B., Ferretti, G., Di Giuseppe, D., Fotovat, A., Halajnia, A., 2018. Leaching behaviour of a sandy soil amended with natural and NH^{4+} and K^{+} saturated clinoptilolite and chabazite. Arch. Agron. Soil Sci. 64, 1142–1151. https://doi.org/10.1080/03650340.2017.1414944.

Faccini, B., Di Giuseppe, D., Malferrari, D., Coltorti, M., Abbondanzi, F., Campisi, T., Laurora, A., Passaglia, E., 2015. Ammonium-exchanged zeolitite preparation for agricultural uses: From laboratory tests to large-scale application in ZeoLIFE project prototype. Period. Miner. 84, 303–321. https://doi.org/10.2451/2015PM0015.

Galamini, G., Malferrari, D., Altimari, F., Orlandi, S., Barbieri, L., 2024. From quarry by-products to a zeolites-based Zn fertilizer with increased resistance to rain leaching. Micro Mesopor. Mat. 379, 113290. https://doi.org/10.1016/j.micromeso.2024.113290.

Govil, S., Van Duc Long, N., Escribà-Gelonch, M., Hessel, V., 2024. Controlled-release fertiliser: Recent developments and perspectives. Ind. Crops Prod. 219, 119160. https://doi.org/10.1016/j.indcrop.2024.119160.

Herencia, J.F., García-Galavís, P.A., Maqueda, C., 2011. Long-Term Effect of Organic and Mineral Fertilization on Soil Physical Properties Under Greenhouse and Outdoor Management Practices. Pedosphere 21, 443–453. https://doi.org/10.1016/S1002-0160(11)60146-X.

Hongsriphan, N., Viratchaiboot, N., Indrasook, P., Hanbuakaeo, S., 2019. Preparation and properties of composite films from poly(butylene succinate), poly(butylene adipate-*co*-terephthalate) and zeolite. Key Eng. Mater. 798, 285–290. https://doi.org/10.4028/www.scientific.net/KEM.798.285.

Houba, V.J.G., Temminghoff, E.J.M., Gaikhorst, G.A., Van Vark, W., 2000. Soil analysis procedures using 0.01 M calcium chloride as extraction reagent. Commun. Soil Sci. Plant Anal. 31, 1299–1396. https://doi.org/10.1080/00103620009370514.

Inglezakis, V., Zorpas, A., Loizidou, M., Grigoropoulou, H., 2005. The effect of competitive cations and anions on ion exchange of heavy metals. Sep. Purif. Technol. 46, 202–207. https://doi.org/10.1016/j.seppur.2005.05.008.

Jarosz, R., Szerement, J., Gondek, K., Mierzwa-Hersztek, M., 2022. The use of zeolites as an addition to fertilisers – a review. Catena 213. https://doi.org/10.1016/j.catena.2022.106125.

Kader, M.A., Senge, M., Mojid, M.A., Ito, K., 2017. Recent advances in mulching materials and methods for modifying soil environment. Soil Tillage Res. 168, 155–166. https://doi.org/10.1016/j.still.2017.01.001.

Kaur, G., Gupta, S., Prakash, V., Rodriguez, R.D., Sheremet, E., Mehta, S.K., Sharma, S., 2024. A comprehensive review of varied applications of modified halloysite nanocomposites. Nano Struct. Nano Objects 39, 101230. https://doi.org/10.1016/j.nanoso.2024.101230.

Khalid, N., Aqeel, M., Noman, A., Rizvi, Z.F., 2023. Impact of plastic mulching as a major source of microplastics in agroecosystems. J. Hazard. Mater. 445, 130455. https://doi.org/10.1016/j.jhazmat.2022.130455.

Klun, U., Krzan, A., 2003. Degradation of polyamides-6 by using metal salts as catalyst. Polym. Adv. Technol. 13 (10-12), 817–822. https://doi.org/10.1002/pat.250.

Krężel, A., Maret, W., 2016. The biological inorganic chemistry of zinc ions. Arch. Biochem. Biophys. Cut. Edge Zinc Biol. 611, 319. https://doi.org/10.1016/j.abb.2016.04.010.
Lateef, A., Nazir, R., Jamil, N., Alam, S., Shah, R., Khan, M.N., Saleem, M., 2016. Synthesis and characterization of zeolite based nano–composite: An environment friendly slow release fertilizer. Microporous Mesoporous Mater. 232, 174–183. https://doi.org/10.1016/j.micromeso.2016.06.020.
Li, X.-Y., Zhou, Q., Wen, Z.-B., Hui, Y., Yang, K.-K., Wang, Y.-Z., 2015. Influence of catalysts used in synthesis of poly(p-dioxanone) on its thermal degradation behaviors. Polym. Degrad. Stab. 121, 253–260. https://doi.org/10.1016/j.polymdegradstab.2015.09.016.
Liu, Y.-M., Liu, D.-Y., Zhao, Q.-Y., Zhang, W., Chen, X.-X., Xu, S.-J., Zou, C.-Q., 2020. Zinc fractions in soils and uptake in winter wheat as affected by repeated applications of zinc fertilizer. Soil Tillage Res. 200, 104612. https://doi.org/10.1016/j.still.2020.104612.
Magalong, J.R., DelaCruz, J., Bumatay, J., Deocaris, C., 2022. PUPAK: parameter estimation, and plot visualization of adsorption kinetic models. https://doi.org/10.32614/CRAN.package.PUPAK..
Malferrari, D., Laurora, A., Brigatti, M.F., Coltorti, M., Di Giuseppe, D., Faccini, B., Passaglia, E., Vezzalini, M.G., 2013. Open-field experimentation of an innovative and integrated zeolitite cycle: Project definition and material characterization. Rend. Lince 24, 141–150. https://doi.org/10.1007/s12210-013-0235-3.
Mansoor, Z., Tchuenbou-Magaia, F., Kowalczuk, M., Adamus, G., Manning, G., Parati, M., Radecka, I., Khan, H., 2022. Polymers use as mulch films in agriculture A review of history problems and current trends. Polymers 14, 5062. https://doi.org/10.3390/polym14235062.
de Mendiburu, F., 2006. Agricolae: Statistical Procedures for Agricultural Research. https://doi.org/10.32614/CRAN.package.agricolae.
Merino, D., Zych, A., Athanassiou, A., 2022. Biodegradable and biobased mulch films: highly stretchable PLA composites with different industrial vegetable waste. ACS Appl. Mater. Interfaces 14 (41), 46920–46931. https://doi.org/10.1021/acsami.2c10965.
Miles, C., DeVetter, L., Ghimire, S., Hayes, D.G., 2017. Suitability of biodegradable plastic mulches for organic and sustainable agricultural production systems. HortScience 52 (1), 10–15. https://doi.org/10.21273/HORTSCI11249-16.
Minichiello, C., Pagliarini, E., Baffoni, L., Di Gioia, D., Ferri, M., Vannini, M., Celli, A., Saccani, A., Sisti, L., 2025. Artichoke bracts and stems residue as active filler for poly(butylene succinate-co-adipate) (PBSA) composites: from agro-waste to a new sustainable material. Polym. Comp. 0, 1–17. https://doi.org/10.1002/pc.70289.
Morante-Carballo, F., Montalván-Burbano, N., Carrión-Mero, P., Espinoza-Santos, N., 2021. Cation Exchange of Natural Zeolites: Worldwide Research. Sustainability 13, 7751. https://doi.org/10.3390/su13147751.
Moreno-Lora, A., Delgado, A., 2020. Factors determining Zn availability and uptake by plants in soils developed under Mediterranean climate. Geoderma 376, 114509. https://doi.org/10.1016/j.geoderma.2020.114509.
Noroozifar, M., Khorasani-Motlagh, M., Naderpour, H., 2014. Modified nanocrystalline natural zeolite for adsorption of arsenate from wastewater: Isotherm and kinetic studies. Micro Mesopor. Mater. 197, 101–108. https://doi.org/10.1016/j.micromeso.2014.05.037.
Noulas, C., Tziouvalekas, M., Karyotis, T., 2018. Zinc in soils, water and food crops. J. Trace Elem. Med. Biol. 49, 252–260. https://doi.org/10.1016/j.jtemb.2018.02.009.
Orgiazzi, A., Panagos, P., Fernández-Ugalde, O., Wojda, P., Labouyrie, M., Ballabio, C., Franco, A., Pistocchi, A., Montanarella, L., Jones, A., 2022. LUCAS Soil Biodiversity and LUCAS Soil Pesticides, new tools for research and policy development. Eur. J. Soil Sci. 73, e13299. https://doi.org/10.1111/ejss.13299.
Pagliarini, E., Totaro, G., Saccani, A., Lancellotti, I., Di Gioia, D., Sisti, L., 2023. Valorization of coffee wastes as plant growth promoter in mulching film production: A contribution to a circular economy. Sci. Total Environ. 871, 162093. https://doi.org/10.1016/j.scitotenv.2023.162093.
Paliaga, S., Badalucco, L., Ciaramitaro, V.C., Chillura Martino, D.F., Gelsomino, A., Kandeler, E., Marhan, S., Laudicina, V.A., 2025. Fertilizer enriched bio-based mulch films increase nitrogen and phosphorus availability and stimulate soil microbial biomass and activity. Appl. Soil Ecol. 211, 106159. https://doi.org/10.1016/j.apsoil.2025.106159.
Parida, M., Shajkumar, A., Mohanty, S., Biswal, M., Nayak, S.K., 2022. Poly(lactic acid) (PLA)-based mulch films: evaluation of mechanical, thermal, barrier properties and aerobic biodegradation characteristics in real-time environment. Polym. Bull. 80 (10), 3649–3674. https://doi.org/10.1007/s00289-022-04203-4.
Priya, E., Sudipta, S., Pradip, M.K., 2024. A review on slow-release fertilizer: Nutrient release mechanism and agricultural sustainability. J. Environ. Chem. Eng. 12, 113211. https://doi.org/10.1016/j.jece.2024.113211.
Pueyo, M., López-Sánchez, J.F., Rauret, G., 2004. Assessment of CaCl2, NaNO3 and NH4NO3 extraction procedures for the study of Cd, Cu, Pb and Zn extractability in contaminated soils. Anal. Chim. Acta 504, 217–226. https://doi.org/10.1016/j.aca.2003.10.047.
Qiu, H., Lv, L., Pan, B.C., Zhang, Q.J., Zhang, W.M., Zhang, Q.X., 2009. Critical review in adsorption kinetic models. J. Zhejiang Univ. Sci. A 10, 716–724. https://doi.org/10.1631/jzus.A0820524.
Sahoo, S., Rout, A.A., 2024. Polylactic Acid (PLA) Film with the incorporation of fruit peel waste: a short review. J. Macromol. Sci. Phys. 63 (2), 61–74. https://doi.org/10.1080/00222348.2023.2251811.
Salama, K., Geyer, M., 2023. Plastic mulch films in agriculture: their use, environmental problems, recycling and alternatives. Environments 10 (10), 179. https://doi.org/10.3390/environments10100179.
Sanders, J.R., El Kherbawy, M.I., 1987. The effect of pH on zinc adsorption equilibria and exchangeable zinc pools in soils. Environ. Pollut. 44, 165–176. https://doi.org/10.1016/0269-7491(87)90001-7.
de Santiago, A., Quintero, J.M., Delgado, A., 2008. Long-term effects of tillage on the availability of iron, copper, manganese, and zinc in a Spanish Vertisol. Soil Tillage Res 98, 200–207. https://doi.org/10.1016/j.still.2008.01.002.
dos Santos Pereira, T., Santos Fernandes, L., Fonseca Souza, C., Faez, R., 2021. Biodegradable enhanced efficiency fertilizer based on biopolymers/zeolites films' assembly. ACS Agric. Sci. Technol. 1, 131–142. https://doi.org/10.1021/acsagscitech.0c00002.
Scopetani, C., Bellabarba, A., Selvolini, G., Martellini, T., Viti, C., Cincinelli, A., 2025. Evaluating additive release from conventional and biodegradable mulch films. Sci. Total Environ. 975, 179294. https://doi.org/10.1016/j.scitotenv.2025.179294.
Serrano-Ruiz, H., Martin-Closas, L., Pelacho, A.M., 2021. Biodegradable plastic mulches: Impact on the agricultural biotic environment. Sci. Total Environ., 141228 https://doi.org/10.1016/j.scitotenv.2020.141228.
Singh, G., Ramadass, K., Sooriyakumar, P., Hettithanthri, O., Vithange, M., Bolan, N., Tavakkoli, E., Van Zwieten, L., Vinu, A., 2022. Nanoporous materials for pesticide formulation and delivery in the agricultural sector. J. Control. Release 343, 187–206. https://doi.org/10.1016/j.jconrel.2022.01.036.
Soulis, S., Triantou, D., Weidner, S., Jana, F., Johannis, S., 2012. Structural analysis of biodegradable low-molecular mass copolyesters based on glycolic acid, adipic acid and 1,4 butanediol and correlation with their hydrolytic degradation. Polym. Degrad. Stabil. 97 (11), 2091–2103. https://doi.org/10.1016/j.polymdegradstab.2012.09.002.
de Sousa, A.G., Ferreira, R.R., Harada, J., Rosa, D.S., 2021. Field performance on lettuce crops of poly(butylene adipate-co-terephthalate)/polylactic acid as alternative biodegradable composites mulching films. J. Appl. Polym. Sci. 138 (11), 50020. https://doi.org/10.1002/app.50020.
de Souza Vieira, L., Stieven Montagna, L., Bernardo da Silva, A.P., Almeida Verginio, G.E., Passador, F.R., 2021. Effect of glassy carbon addition and photodegradation on the biodegradation in aqueous medium of poly (3-hydroxybutyrate-co-3-hydroxyvalerate)/glassy carbon green composites. J. Appl. Polym. Sci. 138 (33), 50821. https://doi.org/10.1002/app.50821.
Steinmetz, Z., Wollman, C., Schaefer, M., Buchmann, C., David, J., Troger, J., Munoz, C., Fror, O., Schaumann, G.E., 2016. Plastic mulching in agriculture. Trading short-term agronomic benefits for long-term soil degradation? Sci. Total Environ. 550, 690–705. https://doi.org/10.1016/j.scitotenv.2016.01.153.
Tang, K.H.D., 2023. Microplastics in agricultural soils in China: Sources, impacts and solutions. Environ. Pollut. 322, 121235. https://doi.org/10.1016/j.envpol.2023.121235.
Venables, W.N., Ripley, B.D., 2002. Modern Applied Statistics with S. Statistics and Computing. Springer New York, New York, NY. https://doi.org/10.1007/978-0-387-21706-2.
Wang, Y., Wang, C., Huang, X., Zhang, Q., Wang, T., Guo, X., 2024. Guideline for modeling solid-liquid adsorption: Kinetics, isotherm, fixed bed, and thermodynamics. Chemosphere 349, 140736. https://doi.org/10.1016/j.chemosphere.2023.140736.
Wennmacher, J.T.C., Li, T., Zaubitzer, C., Gemmi, M., Mugnaioli, E., Gruene, T., van Bokhoven, J.A., 2020. Heterogeneity of nano-sized zeolite crystals. Microporous Mesoporous Mater. 294, 109897. https://doi.org/10.1016/j.micromeso.2019.109897.

Wu, F.-C., Tseng, R.-L., Juang, R.-S., 2009. Initial behavior of intraparticle diffusion model used in the description of adsorption kinetics. Chem. Eng. J. 153, 1–8. https://doi.org/10.1016/j.cej.2009.04.042.

Younas, N., Fatima, I., Ahmad, I.A., Ayyaz, M.K., 2023. Alleviation of zinc deficiency in plants and humans through an effective technique; biofortification: A detailed review. Acta Ecol. Sin. 43, 419–425. https://doi.org/10.1016/j.chnaes.2022.07.008.

Yu, Y., Velandia, M., Hayes, D.G., DeVetter, L.W., Miles, C., Flury, M., 2024. Biodegradable plastics as alternatives for polyethylene mulch films. Adv. Agron. 183, 121–192. https://doi.org/10.1016/bs.agron.2023.10.003.

Zhang, B., Zhang, K., Jia, X., Liu, Y., Zhang, X., Yu, H., Liu, J., Wang, Q., Waterhouse, G.I.N., Xie, J., Xu, J., 2025. Biodegradable poly (butylene adipate-co-terephthalate)/polylactic acid mulching films containing glufosinate ammonium-loaded layered double hydroxide: Enhanced performance, herbicidal performance and extended functional life. Int. J. Biol. Macromol. 307, 141519. https://doi.org/10.1016/j.ijbiomac.2025.141519.

Zhang, H., Shu, D., Zhang, J., Liu, X., Wang, K., Jiang, R., 2024. Biodegradable film mulching increases soil microbial network complexity and decreases nitrogen-cycling gene abundance. Sci. Total Environ. 933, 172874. https://doi.org/10.1016/j.scitotenv.2024.172874.

Zhang, S., Yang, M., Meng, S., Yang, Y., Li, Y.C., Tong, Z., 2022. Biowaste-derived, nanohybrid-reinforced double-function slow-release fertilizer with metal-adsorptive function. Chem. Eng. J. 450, 138084. https://doi.org/10.1016/j.cej.2022.138084.